Organization of Dispersions of a Linear Diblock Copolymer of Polystyrene and Poly(ethylene oxide) at the Air−Water Interface

P. F. Dewhurst, M. R. Lovell, J. L. Jones, and R. W. Richards*

Interdisciplinary Research Centre in Polymer Science and Technology, Department of Chemistry, University of Durham, Durham, DH1 3LE, U.K.

J. R. P. Webster

ISIS Facility, Rutherford Appleton Laboratory, Chilton, Didcot, Oxon, OX11 0QX, U.K.

Received February 25, 1998; Revised Manuscript Received August 3, 1998

ABSTRACT: The spontaneous adsorption of a highly monodisperse associative block copolymer, poly(styrene-*b*-ethylene oxide) from bulk aqueous solution to the air−solution interface has been studied using static surface tensiometry and specular neutron reflectometry. The bulk association behavior of this polymer has been examined using light scattering, and the critical micelle concentration (CMC) was found to be $(3.5 \pm 0.4) \times 10^{-5}$ g mL^{-1}. Hydrodynamic radii obtained by quasi-elastic light scattering suggest a closed association model for the aggregation and a hydrodynamic radius of 165 as observed for dispersion concentrations greater than 0.1 mg mL^{-1}. Static surface tension data showed that the copolymer displayed surface activity even at very low bulk concentrations. Selected concentrations have been investigated in detail, coinciding with specific regions of the closed association regime. Neutron reflectometry was used to determine the structure normal to the air−water interface at these selected concentrations. Well-below the CMC, the copolymer is in a self-similar adsorbed layer, which we attribute to surface micellization. At the CMC the surface excess of the copolymer is increased and the ethylene oxide segments explore deeper into the subphase and become detectable by neutron reflectometry. At increasing concentrations above the CMC "structuring" of the polystyrene-rich regions occurs within the space explored by the poly(ethylene oxide) chains. The layering of the hydrophobic polystyrene blocks is considered a result of clustering of spherical micelles in the surface region, the onset of which coincides with an apparent phase transition in the surface tension variation with bulk concentration data.

Introduction

When dispersed in a selective solvent for one of the blocks, linear diblock copolymers form micelles of well-defined morphology above a critical micelle concentration (CMC) due to the inherent amphiphilicity of the copolymer. The same property also imparts surface activity to such copolymers. The micellization behavior makes block copolymers ideal candidates for dye transportation and, potentially, as drug carrier systems. Their surfactant properties make them useful as colloid stabilizers, antifoaming agents, and emulsifiers. Most studies have concentrated on only one aspect of this rich behavior spectrum: micellization,[1−10] the spread monolayer,[9−13] or adsorption from solution onto solid surfaces.[14−23] Few have addressed adsorption from solution to the air−water interface,[24,25] and none to our knowledge have examined how the structure of the adsorbed interfacial layer relates to the nature of the copolymer in solution (i.e., monomolecular or micellar).

We discuss here the organization of a poly(styrene-*b*-ethylene oxide) copolymer at the air−water interface as a function of the concentration of a copolymer dispersed in the aqueous phase. These data for the near-surface organization are complemented with investigations of the surface tension by classical methods and the micelle size in the bulk dispersion. The paper is organized in the following way. First, the synthesis of the copolymer is outlined together with the results of the copolymer characterization. Second, the copolymer aggregation behavior in aqueous solution is then addressed followed by the results of surface adsorption experiments (surface tensiometry) and investigations of the near-surface organization by neutron reflectometry (NR).

Theoretical Background

The key principle of reflectometry is to deliver a well-collimated beam of neutrons of known wavelength λ onto a macroscopic surface at a glancing angle θ and measure the reflectivity, R, as a function of scattering vector Q (defined as $(4\pi/\lambda) \sin \theta$). The specular reflectivity $R(Q)$ is then interpreted in terms of the scattering length density profile perpendicular to the surface. Surface structural information is obtained by comparing the measured $R(Q)$ with that calculated for theoretical models. There are two theoretical approaches to calculating $R(Q)$. One is the exact optical matrix method derived from optics[26,27] and the other is a good approximation valid when Q is not too small (i.e., total reflection conditions are not approached (generally $Q > 0.03$ Å^{-1}).[28,29] Since both approximate and exact methods are used here, we discuss each in turn briefly starting with the approximate equations. The kinematic approximation $R(Q)$, after correction for the incoherent background, can be defined as

$$R(Q) = \frac{16\pi^2}{Q^4}|\hat{\rho}'(Q)|^2 \qquad (1)$$

In this expression $\rho'(Q)$ is the one-dimensional Fourier transform of the gradient of the average scattering length density, $\rho(z)$, with distance normal to the inter-

* To whom correspondence should be addressed.

10.1021/ma9802935 CCC: $15.00
Published on Web 10/10/1998

face z:

$$\tilde{\rho}(Q) = \int_{-\infty}^{\infty} \frac{d\rho(z)}{dz} \exp(-\mathbf{i}Qz)\, dz \qquad (2)$$

The expression $|\rho'(Q)|^2$ in eq 1 has been called the film factor $f(Q)$ (units: Å^{-4}) since the function contains all the information regarding the surface "film" but does not have the underlying Q^{-4} dependent decay of reflectivity. Taking eqs 1 and 2 together shows that the reflectivity of an interface in the kinematic approximation is determined solely by the presence of scattering length density *changes* normal to the interface. The kinematic approximation does not take account of the effect of the finite surface roughness/diffuseness but rather assumes a perfectly flat and sharp interface. The benefits obtained through both ease of use of the kinematic approximation and the opportunity to determine uniquely the interfacial structure by using deuterium labeling to change ρ(z) surpass the inability of the approximation to deal with roughness/diffuseness.

The exact reflectivity equations define $R(Q)$ for all Q. The equations arise from standard multilayer optical methods[26] and are termed dynamical, but this approach can only be extended easily for three or four discrete layers.[30] Beyond this level of complexity, a general dynamical solution must be adopted. The method described by Born and Wolf[26] does not take account of interfacial roughness/diffuseness; therefore, Abélès matrix method is usually adopted more[27] in which the reflectance is modified by a root-mean-square Gaussian roughness factor.

Reflectivity Data Analysis

The most common approach used to analyze reflectivity data is to assume a model scattering length density profile consisting of a series of discrete homogeneous layers of defined scattering length density and thickness. Least-squares minimization techniques are then employed to vary the parameters of the layers in order to obtain a best fit to the reflectivity data using optical matrix methods of calculating $R(Q)$. This "slab" model fitting procedure can be highly subjective, since the best-fit solution chosen is maybe just one of several possibilities. Moreover, this method can be extremely difficult and time-consuming when the scattering length density profiles are complicated. We have therefore used the more objective model independent (MI) method of Pedersen.[31,32] This method uses the dynamical equations, and no correction for multiple scattering from highly reflective specimens is necessary. In the MI method only the scattering length densities of the upper and lower bulk phases need be known, together with a value for the finite depth of the interface to be modeled and a starting estimate of the mean scattering length density prior to fitting. For our data analysis we have chosen the mean scattering length density to be equal to that of the bulk subphase, and thus no a priori structure is imparted to the interface prior to fitting. In the MI analysis the scattering length density variation is modeled by a series of damped cubic splines, and the result is the fitted scattering length density profile itself $\rho(z)$ rather than parameters that describe the composition distribution directly. Caution still needs to be exercised because the fitted $\rho(z)$ profile may not be a unique solution. The $\rho(z)$ profile obtained by the MI analysis allows estimates for initial structural parameters to be made that can be used in a more quantitative analysis technique. To describe the surface organization quantitatively, and to obtain unique $\rho(z)$ profiles, the partial-structure factor (PSF) analysis method of Thomas et al.[33−35] has also been employed. The PSF analysis utilizes the kinematic approximation to determine uniquely the experimental number-density profiles of each component i, n_i, as a function of the scattering vector Q, $n_i(Q)$, rather than in real space as a function of z, $n_i(z)$.

An equivalent kinematic reflectivity expression to that of eq 1 is

$$R(Q) = \frac{16\pi^2}{Q^2} \left| \int_{-\infty}^{\infty} \rho(z) \exp(-\mathbf{i}Qz)\, dz \right|^2 \qquad (3)$$

in which the scattering length density $\rho(z)$ is defined as

$$\rho(z) = \sum_{i=1}^{k} b_i n_i(z) \qquad (4)$$

In eq 4, b_i is the coherent scattering length of component i, the total number of components in the surface under investigation being k. Here $k = 3$ since we are interested in styrene (S) segments, ethylene oxide (E) segments, and water (W) molecules; thus,

$$\rho(z) = b_S n_S(z) + b_E n_E(z) + b_W n_W(z) \qquad (5)$$

Substituting the full expression for $\rho(z)$ given in eq 5 into eq 3 and rearranging leads to

$$\frac{R(Q)Q^2}{16\pi^2} = b_S{}^2 \hat{n}_S{}^2(Q) + b_E{}^2 \hat{n}_E{}^2(Z) + b_W{}^2 \hat{n}_W{}^2(Q) + 2b_S b_E \hat{n}_S(Q)\hat{n}_E(Q) + 2b_S b_W \hat{n}_S(Q)\hat{n}_W(Q) + 2b_E b_W \hat{n}_E(Q)\hat{n}_W(Q) \qquad (6)$$

where $\hat{n}_i(Q)$ is the Fourier transform of $n_i(z)$. Equation 6 is rewritten in terms of the partial-structure factors as

$$\frac{R(Q)Q^4}{16\pi^2} = b_S{}^2 Q^2 h_{SS}(Q) + b_E{}^2 Q^2 h_{EE}(Q) + b_W{}^2 Q^2 h_{WW}(Q) + 2b_S b_E Q^2 h_{SE}(Q) + 2b_S b_W Q^2 h_{SW}(Q) + 2b_E b_W Q^2 h_{EW}(Q) \qquad (7)$$

In general, $h_{ii}(Q)$, the self-partial-structure factors, contain compositional and dimensional information for the individual component i only and the cross-partial-structure factors $h_{ij}(Q)$ have information on the separations of components i and j. The six partial-structure factors are obtained by a simultaneous solution of eq 7 for six systems of identical chemical composition but different scattering length (contrast) combinations. The range of contrasts is obtained by exploiting the large difference in the scattering length between hydrogen ($b_H = -3.74 \times 10^{-5}$ Å) and deuterium ($b_D = 6.67 \times 10^{-5}$ Å) via combinations of hydrogenous and deuterated components (see later). The experimental PSFs can then be modeled using Fourier transforms of idealized distributions for each component (e.g., uniform number density over a finite distance). Prior to substitution in eq 7, reflectivity profiles obtained from highly reflecting

surfaces (i.e., those containing D_2O) must first be corrected using Crowley's method.[36]

Experimental Section

Copolymer Synthesis. It is essential that the complete range of deuterium labeling available is explored in the neutron reflectivity data so that the most complete description of the copolymer surface organization can be made via PSF analysis. Consequently, the styrene−ethylene oxide diblock copolymer was prepared with all possible combinations of deuterated (d) and hydrogenous (h) segments (i.e. dPS−dPEO, dPS−hPEO, hPS−dPEO, and hPS−hPEO). To maintain constant chemical composition throughout all contrasts, the PS and PEO blocks were prepared as reproducibly as possible (molecular weight, composition, and polydispersity) using the method of Jialanella et al.[37] The PS blocks and the linear diblock copolymers were analyzed by size-exclusion chromatography and ^{13}C NMR using chloroform as the solvent in both techniques.

Copolymer Solution Behavior. The CMC of the hPS−hPEO copolymer dispersed in water was determined by light scattering. Samples were prepared by adding a known amount of copolymer to 50 mL of ultrapure water (UHQ water, resistivity >18 MΩcm) and then left to equilibrate for at least 24 h with occasional shaking. Each dispersion was filtered directly into sample cells through membrane filters with a pore size of 0.22 μm. An Ar^+ laser illuminated each sample with vertically polarized light with a wavelength (in vacuo) of 488 nm and a power of 75.2 mW. The scattered intensity at 90° to the incident beam was collected. Samples were left to equilibrate for several minutes prior to collecting data, equilibrium being indicated when no further change in the scattered light intensity rate was noted. For each sample the average scattered intensity was determined from repeated measurements. Homodyne autocorrelation functions were recorded and analyzed to provide the hydrodynamic radius of the scattering particles. Measurements were repeated after 24 h to ensure that filtration had not destroyed micelles that slowly reformed. No difference in either average scattered intensity or average particle diameter was observed. This procedure was repeated on the dPS−dPEO copolymer to verify that deuteration had no influence on the CMC or micelle size.

Surface Adsorption Behavior. *Surface Tension Measurements.* Copolymer dispersions in water were prepared by adding a known mass of the hydrogenous copolymer to a known volume of UHQ water and allowing the copolymer to disperse for at least 24 h. The surface tension recorded to an uncertainty of ±1 mN m^{-1} at 295 ± 1 K was measured using a NIMA ST900 surface tensiometer (Nima, Coventry, England). For the lowest concentration dispersion investigated, approximately 30 min was required to reach the equilibrium surface tension, presumably due to the finite time required for the copolymer to diffuse from bulk to the surface and rearrange into the equilibrium conformation at the surface. For the higher concentration samples, the equilibration time seemed to be less than the time required to wet the plate fully, equilibrium readings being achieved in under 1 min.

Neutron Reflectometry Experiments. The SURF reflectometer at the ISIS facility, Rutherford Appleton Laboratory, U.K., was used to collect specular neutron reflectivity data. Six combinations of the copolymer and aqueous phase were used so that the complete range of neutron contrasts was explored. The six contrasts chosen were dPS−dPEO/NRW, dPS−hPEO/NRW, hPS−dPEO/NRW, hPS−hPEO/D_2O, dPS−hPEO/D_2O, and hPS−dPEO/D_2O, where NRW denotes null reflecting water (ca. 11:1 H_2O:D_2O w/w). Assessment of the in-plane structure was attempted by performing off-specular neutron reflectivity on the most concentrated dispersion of the dPS−dPEO/NRW combination. No evidence of diffuse reflectivity was observed, and thus we could make no estimation of the existence of any in-plane organization.

Each dispersion was placed in one of five parallel poly(tetrafluoroethylene) troughs that each held 25 cm^3 of the sample with the long axis of the trough in the direction of the incident neutron beam. Reflectivity data were collected for two angles of incidence on the dispersion surface such that the range of Q explored was from 0.025 to 0.65 $Å^{-1}$.

Table 1. Copolymer SEC Characterization Data

	styrene block[a]		total copolymer[b]	
copolymer	$\overline{M_n}$/g mol^{-1}	$\overline{M_w}/\overline{M_n}$	$\overline{M_n}$/g mol^{-1}	$\overline{M_w}/\overline{M_n}$
dPS−dPEO	1280	1.10	7580	1.05
dPS−hPEO	1280	1.10	6670	1.05
hPS−dPEO	1430	1.07	8180	1.04
hPS−hPEO	1430	1.07	8490	1.04

[a] PS block vs PS standards. [b] Copolymer vs PEO standards.

Table 2. Copolymer Composition in Mole Percent Styrene

copolymer	^{13}C NMR	mass balance
dPS−dPEO	7.2	7.8
dPS−hPEO	7.4	7.9
hPS−dPEO	7.0	7.1
hPS−hPEO	7.7	7.7

Results

Copolymer Characterization. Number-average molecular weights and polydispersity of the PS blocks and the copolymers are given in Table 1; copolymer compositions were obtained using ^{13}C NMR. A composition determined from a mass balance of the synthesis procedure (the ratio of the mass of the styrene monomer over the total mass of monomers of styrene and ethylene oxide used) was also calculated. These compositions are given in Table 2 in terms of the mole percentage styrene repeat unit (mol % of S) in the copolymer. The mol % of S data determined by ^{13}C NMR experiments and the simple mass-balance calculation agree well, the average value being 7.5 ± 0.4. With respect to the absolute content of PS, the copolymers containing dPS blocks have an average of 11 ± 1 styrene units calculated from the $\overline{M_n}$ and $\overline{M_w}/\overline{M_n}$ values of Table 1, column 1), whereas the hPS blocks contain 14 ± 1 styrene units. The average styrene segment content is 13 ± 1, implying a PEO degree of polymerization of 163 ± 6; thus, the average copolymer formula is $(C_8H(D)_8)_{13}(C_2H(D)_4O)_{163}$.

Copolymer Dispersion Behavior. Hydrodynamic radii determined by light-scattering size analysis are shown in Figure 1 as a function of copolymer concentration. For concentrations less than approximately 4.0 × 10^{-5} g mL^{-1} (to the left of B, Figure 1) the average particle diameter is very small and the copolymer is present as isolated chains (unimers) in solution. At a concentration of approximately 5 × 10^{-5} g mL^{-1} the particles abruptly increase in size, eventually reaching an asymptotic radius of ∼160 Å at point C. We associate this region with the formation and growth of copolymer micelles in the bulk solution in equilibrium with copolymer unimers. Other studies have shown that PS−PEO copolymers micellize readily in aqueous solution, and the spherical micelles have a solvent-free PS core surrounded by a solvent-swollen corona of PEO chains.[2−8] We have not, however, found any evidence of micelle aggregation to form the larger aggregates reported by some workers.[2−4,8] At 10^{-3} g mL^{-1} (point D) the average particle size has not changed significantly from that at 10^{-4} g mL^{-1}, but the size polydispersity has decreased. The average particle radius for dPS−dPEO and hPS−hPEO after equilibration for 24

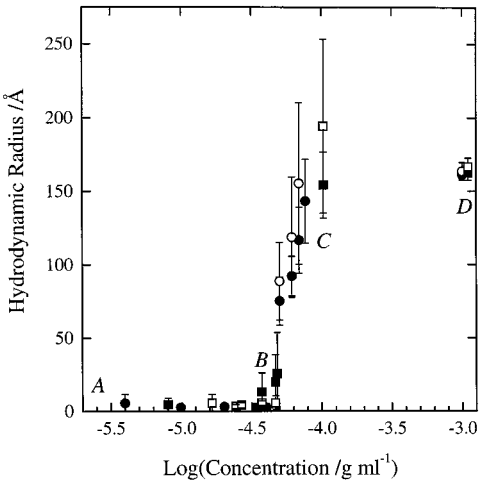

Figure 1. Hydrodynamic radius at 298 K of dispersed particles in water as a function of copolymer concentration. Fully hydrogenous copolymer (○) immediately after filtration and (●) after 24 h. Fully deuterated copolymer (■) immediately after filtration and (□) after 24 h. Points marked A (2.5×10^{-6} g mL^{-1}), B (3.5×10^{-5} g mL^{-1}), C (10^{-4} g mL^{-1}), and D (10^{-3} g mL^{-1}) are the concentrations used for neutron reflectometry.

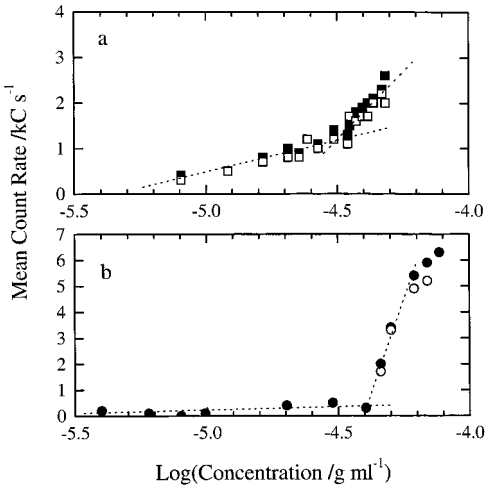

Figure 2. Mean count rate of scattered light intensity for copolymer dispersions as a function of concentration at 298.0 ± 0.1 K. (a) Fully deuterated copolymer and (b) fully hydrogenous copolymer. Symbols as for Figure 1.

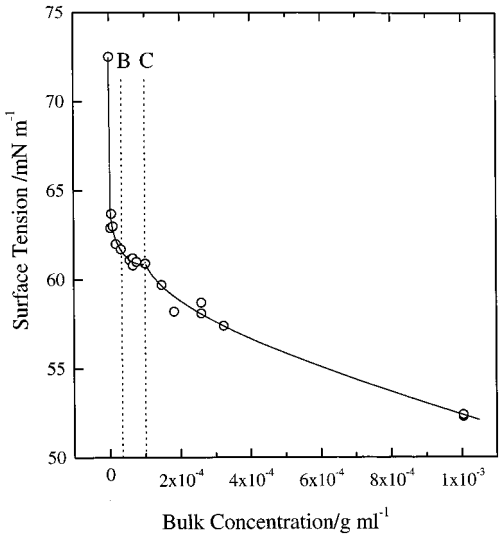

Figure 3. Surface tension, γ_0, as a function of dispersion concentration at 295 ± 1 K. B and C are the concentrations defined in Figure 1, the CMC (3.5×10^{-5} g mL^{-1}) and 10^{-4} g mL^{-1}, respectively. The solid lines are guides to the eye.

h are 167 ± 6 and 163 ± 6 Å, respectively, and agree well with each other. The average hydrodynamic radius for the micelles of all varieties of the PS−PEO copolymer is 165 ± 6 Å. The observation of an asymptotic micelle size is characteristic of formation by a closed association process.[38] Once the maximum micelle size has been reached, a further increase in the copolymer concentration results in the formation of more micelles of the same size. The concentration of unimers in this model remains roughly constant at the CMC, which is approximately 4.5×10^{-5} g mL^{-1}. Deuteration of the copolymer does not noticeably affect the CMC.

The size of the error bars in Figure 1 give an indication as to the size polydispersity of all species in solution (micelles and unimers) at each concentration studied and reflects the ratio of micelles to unimers. Below the CMC virtually no aggregates exist and the size polydispersity of copolymer species is small. Well-above the CMC virtually all the copolymer is present as micelles (e.g., at 10^{-3} g mL^{-1} approximately 96% of copolymer exists in micellar aggregates) and again the size polydispersity is small. Between these extremes, however, the proportions of unimers and micelles are similar (e.g., at 10^{-4} g mL^{-1} about 65% of copolymer exists in micellar aggregates), and therefore the polydispersity in size is large.

To confirm the value for the CMC, the intensity of scattered light was plotted as a function of copolymer concentration. It is possible that micelles may form at copolymer concentrations less than 4.5×10^{-5} g mL^{-1} but are too dilute to produce a measurable correlation function. The scattered intensity is usually a much more sensitive measure of the CMC and these data are plotted in Figure 2 as the mean count rate versus the copolymer concentration. Figure 2a corresponds to dPS−dPEO and Figure 2b to hPS−hPEO, both dispersed in water. The CMCs for these systems were identified as the concentration where the marked increase in scattered intensity occurred. In the case of dPS−dPEO this is at approximately 3.2×10^{-5} g mL^{-1} whereas for hPS−hPEO the CMC is at approximately 3.9×10^{-5} g mL^{-1} (the lines in Figures 2a and 2b are guides to the eye and are not linear fits to the data). The discrepancy between the two CMCs may be due to small differences in composition and block molecular weight of the two copolymers, the average CMC being $(3.5 \pm 0.4) \times 10^{-5}$ g mL^{-1}. The light-scattering data were insufficient to determine the aggregation number of the micelles, but PS−PEO copolymers of a similar composition and molecular weight have been reported as having aggregation numbers of approximately 60−80.[4,5,7]

Surface Adsorption Behavior. A plot of the static surface tension, γ_0, versus bulk copolymer concentration is shown in Figure 3. The solid line is a guide to the eye. The vertical lines marked B and C correspond respectively to points B and C in Figure 1 (i.e., the CMC and the point at which the micelles attain their asymptotic hydrodynamic radius). The uncertainty in each datum point is estimated to be ±1 mN m^{-1} but error bars are omitted from Figure 3 for clarity. For concentrations less than the CMC, γ_0 decreases dramatically with increasing concentration, indicative of copolymer

adsorption to the surface. From this initial region of Figure 3 it is clear that only very small amounts of the copolymer, $\sim 10^{-6}$ g mL^{-1}, are required to display significant surface activity. At the CMC (line B) γ_0 is 61.5 mN m^{-1}. Between lines B and C γ_0 changes by only 0.5 mN m^{-1} for a 3-fold increase in concentration. The trend in the surface tension behavior at all concentrations up to line C is qualitatively consistent with that determined by others.[24] Nakamura et al.[24] have investigated a range of PS−PEO block copolymers of a constant relative composition but different molecular weight, and a range of similar copolymers of constant PS block molecular weight but with different PEO block lengths. A feature of the surface tension variation with concentration was the observation of a plateau value of γ_0 over a finite range of copolymer concentrations. The value of the plateau surface tension and the concentration range over which it was observed depended on both the copolymer composition and molecular weight. The plateau in γ_0 and its concentration range observed here are consistent with the results of Nakamura et al.

The third region of interest in Figure 3 is for concentrations $>10^{-4}$ g mL^{-1}; the surface tension again decreases with increasing copolymer concentration, but the fall is not as dramatic as in the first region. Nakamura et al.[24] do not explore a sufficiently high enough concentration of their copolymers to observe a similar region. Such kinks in associated surface pressure versus area isotherms for spread polymer films are usually allied with phase transitions in the spread monolayer under investigation. The kink in this case coincides with the concentration at which the bulk micelles reach their asymptotic size. We discuss this "phase transition" later.

Surface Structure. From the light-scattering analysis and the surface tensiometry results, four concentrations of the copolymer were chosen for investigation by NR; 2.5×10^{-6}, 3.5×10^{-5}, 1.0×10^{-4}, and 1.0×10^{-3} g mL^{-1}, corresponding to points A−D in Figure 1. At point A the bulk concentration is very much less than the CMC and the unimers of the copolymer should thus diffuse to the surface and rearrange to the equilibrium conformation. At point B the copolymers are just at the point of aggregation in the bulk phase but most remain as unassociated unimers. At point C bulk micelles of the asymptotic size are present in roughly the same quantity as unimers. At point D the bulk phase micelles are vastly in excess. Between points B and D the copolymer in the surface excess layer may have one of two extreme arrangements.

(1) The surface-adsorbed layer may be composed entirely of unassociated unimers since these are still present in solution even at total concentrations well in excess of the CMC.

(2) Surface microphase separation occurs at a specific concentration that has been termed the critical surface micelle concentration, CSMC.[22] Reflectivity profiles were obtained for the four concentrations listed above at each of the six combinations of copolymer and dispersion media given earlier.

The background was subtracted from all reflectivity data, this background being estimated from the reflectivity with $0.4 \leq Q/\text{Å}^{-1} \leq 0.65$, and the data were first analyzed in the film factor, $f(Q)$, form. The $f(Q)$ format allows differences between the profiles to be seen more effectively and the six $f(Q)$ plots for 10^{-3} g mL^{-1} (point D) are presented in Figure 4. The profiles obtained from

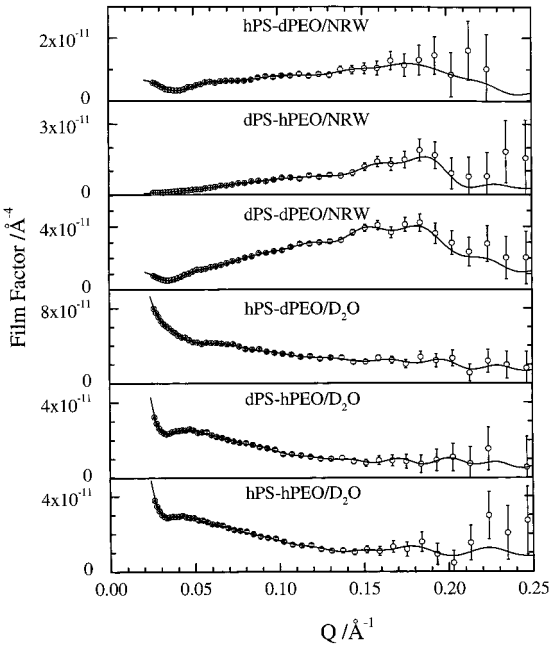

Figure 4. Film factor, $f(Q)$ vs Q data (○) and fits from model independent analysis (—) for all H/D combinations used at a copolymer bulk concentration of 10^{-3} g mL^{-1}.

the other concentrations studied display the same salient features as those in Figure 4 (i.e. an observable maximum in the region $0.15 < Q/\text{Å}^{-1} < 0.25$ for the samples dispersed in NRW) and a general trend of decay of $f(Q)$ for the samples dispersed in D_2O. These general differences between the NRW and D_2O data sets are attributable to the different scattering length densities of the bulk subphase (NRW or D_2O).

Model Independent Fitting. The lines through each data set of Figure 4 are fits obtained using the MI method in conjunction with the exact dynamic reflectivity equations. Trial and error fitting of the reflectivity data sets using interfacial depths ranging from 50 to 400 Å determined that all profiles could be fitted adequately using a depth of 250 Å with 35 splines. The resultant scattering length density profiles obtained are shown in Figure 5 as a function of depth, z. The D_2O-dispersed systems have scattering length density profiles governed mainly by the solvent depth profile as expected. The NRW dispersed systems give a qualitative picture of where the copolymer is situated with respect to the solution surface since there is no contribution to the reflectivity from the NRW. These three profiles display a region, 20−30 Å in depth, at the dispersion surface where most of the copolymer appears to be situated. Assuming that all hydrogenous blocks have essentially zero scattering length density, it appears that both S and EO segments occupy the same surface region at the immediate air−water interface. Quantitative analysis is required to obtain the relative amounts of each, however. Beyond this initial region the profile of the dPEO-containing polymers display a "tail" extending into the bulk solution, clearly indicative of the PEO penetrating to greater depths. Note that there appears to be **no** PEO present in detectable amounts for depths greater than approximately 200 Å. At the lower concentrations studied the scattering length density profiles all show a similar region of 20−30 Å at the surface containing both S and EO segments, although the amplitude of the peak depends on the

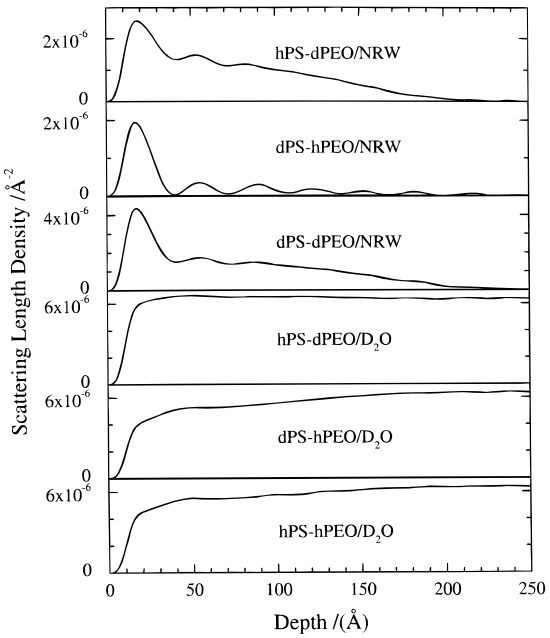

Figure 5. Scattering length density profiles as a function of depth, from the model independent analysis of data for the same copolymer concentration as in Figure 4.

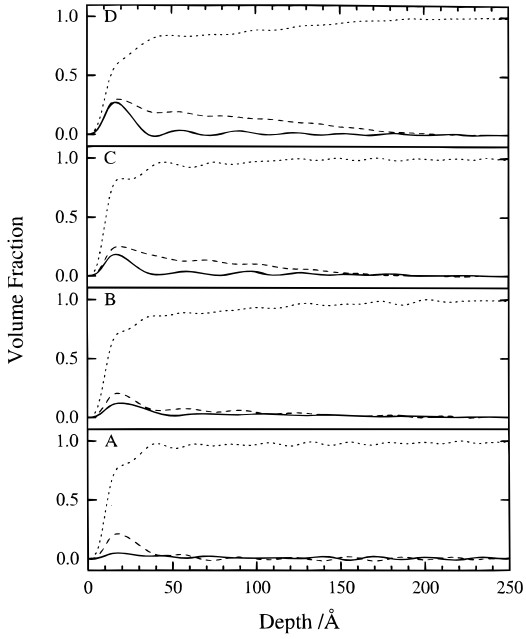

Figure 6. Volume fraction distribution for each component as a function of depth into the subphase. (A) 2.5×10^{-6} g mL^{-1}; (B) 3.5×10^{-5} g mL^{-1} (the CMC); (C) 10^{-4} g mL^{-1}; (D) 10^{-3} g mL^{-1}; (—) styrene; (- - -) ethylene oxide; (···) water.

copolymer concentration. The extended tail region due to PEO is not present in the data for the lowest concentration used (2.5×10^{-6} g mL^{-1}), and only just evident in the data collected at the CMC.

Although eq 5 can be used to calculate the number density of each species normal to the surface, the volume fraction distribution is more useful; this volume fraction distribution is shown in Figure 6. In general, as the bulk concentration increases, so does the volume fraction of S and, albeit to a much lesser extent, EO in the first 50 Å of the surface region. Furthermore, the fraction of EO forming a tail region also increases as a function of increasing concentration. The S and EO

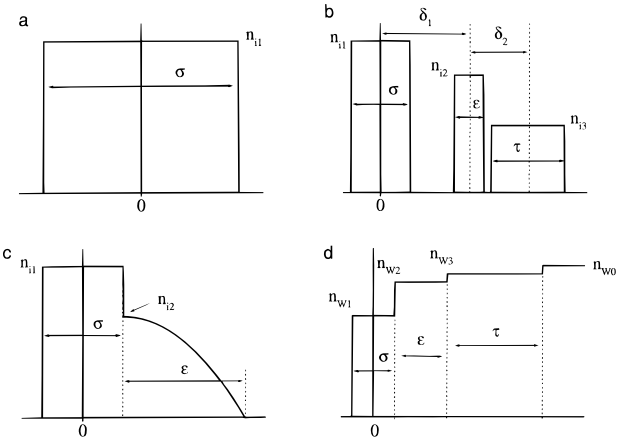

Figure 7. The idealized distributions used to calculate the partial-structure factors. (a) single uniform polymer layer (S and EO segments); (b) triple uniform S layers; (c) uniform-parabolic EO distribution; (d) triple uniform water distribution. The origins do not correspond to the air−water interface.

distributions seem to coexist in the same spatial region because the peak maxima for S and EO all occur at a depth of 18 ± 1 Å.

The general shapes of the individual volume fraction profiles are valid, but the small undulations present are artifacts of the fitting method. The MI fitting method used to obtain the data in Figures 4−6 expresses the component distributions in terms of cubic β-splines. The sum of these basis functions is undulatory and imparts a similar appearance to the scattering length density profiles and the resultant number density and volume fraction profiles. This has been discussed by Pedersen,[31] and subsequently by Pedersen and Hamley,[32] where the authors compare the scattering length density profiles obtained from model independent fits to the original simulated profiles. To summarize, the overall shape of density and volume fraction profiles are acceptable, but the "fine-detail" of the model independent profiles should not be automatically considered as real. This accounts for the fact that some of the density profiles show regions where the volume fraction is a small negative value. In reality, these values correspond to a volume fraction of zero because the profiles undulate randomly about $\phi_i(z) = 0$.

Partial-Structure Factor Analysis. The undulations inherent in the MI fitting may mask real variations in the volume fraction as a function of depth. To determine whether this was the case, we used the kinematic approximation to analyze the reflectivity data as developed by Thomas et al.[33−35] Interpretation of the partial-structure factors obtained has been carried out using popular models of the organization of molecules at an interface (i.e., uniform layers and Gaussian distributions).[34] The near-surface water layer has been modeled either as a single uniform layer or a hyperbolic tangent number-density profile.[34] Additionally, on the basis of the MI volume fraction profiles for EO and water, two other models have been used. Figure 6 suggests that the EO distribution consists of a uniform layer followed by a parabolic decay, which we denote uniform-parabolic. The model for the near-surface water distribution is an extension of the single uniform layer to three single uniform layers, denoted triple uniform. Schematic sketches of these distributions, as well as those used for the S component distributions, are shown in Figure 7. The pertinent information required to define these

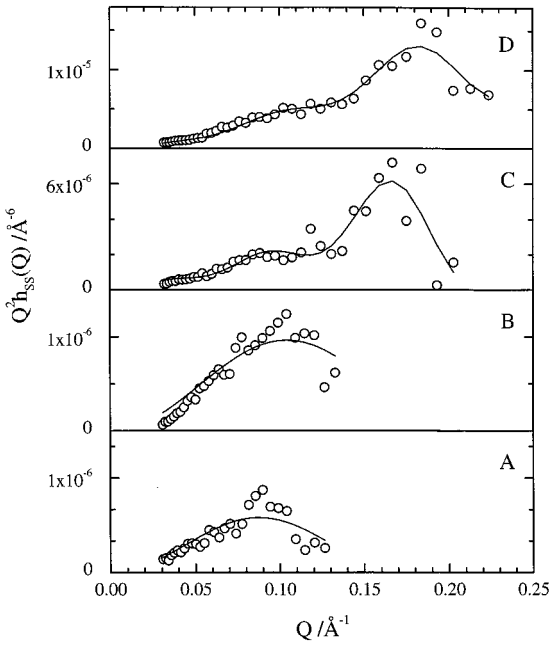

Figure 8. $Q^2h_{SS}(Q)$ as a function of Q, and the best fits (—) obtained using the idealized partial-structure factor for the single uniform layer (A and B) and the triple uniform layers (C and D). A−D indicate the four concentrations selected.

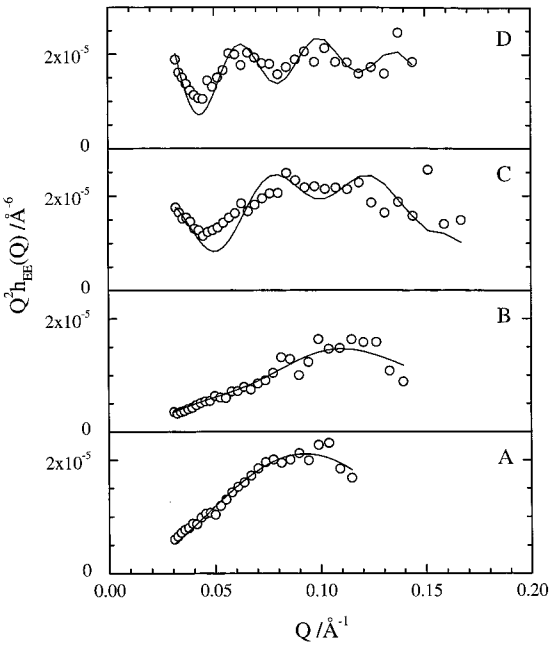

Figure 9. $Q^2h_{EE}(Q)$ as a function of Q, and the best fits (—) obtained using the idealized partial-structure factor for the single uniform layer (A) and the uniform-parabolic distribution (B, C, and D). A−D refer to the four concentrations selected.

distributions (e.g., thickness and number density of species) is included in Figure 7. For use in fitting to partial-structure factor data, it is the Fourier transforms of these number-density distributions that are required and these are given in the Appendix. The self-partial-structure factors and the fits to them are shown in Figures 8−10; the parameters obtained from the fits are listed in Tables 4−6.

Styrene Self-Partial-Structure Factors. The data points for the lowest copolymer concentration studied (Figure 8A) are scattered as a result of the very low reflectivity contribution of the styrene segments due to their low

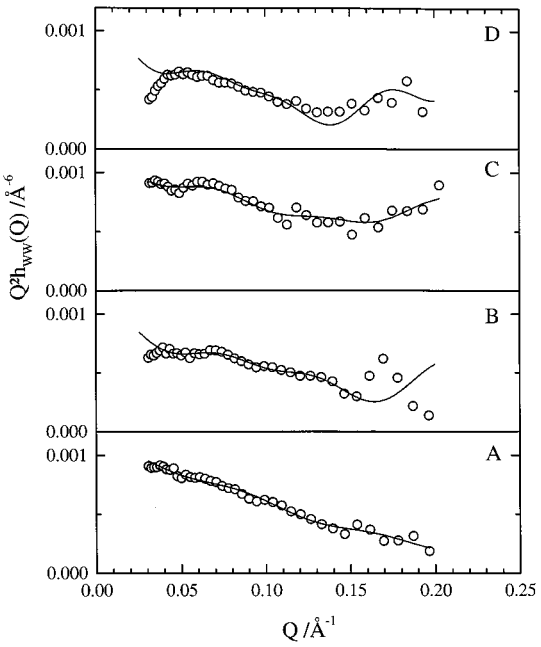

Figure 10. $Q^2h_{WW}(Q)$ as a function of Q for the four copolymer concentrations used, and the best fits (—) obtained using the idealized partial-structure factor for triple uniform solvent layers.

Table 3. Scattering Lengths of Components in Dispersions

component	segment formula	$b/10^{-4}$ Å
styrene	C_8H_8	2.33
	C_8D_8	10.66
ethylene oxide	C_2H_4O	0.42
	C_2D_4O	4.58
water	NRW	0
	D_2O	1.91

concentration. The data have been truncated at $Q = 0.13$ Å^{-1} because the background subtraction from the original reflectivity profiles produced randomly scattered data beyond this point. A good fit using the single uniform polymer layer of Figure 7 was found. The fit was obtained employing eq A4 given in the Appendix by allowing the number density of segments, n_{i1}, and the distribution width, σ, to vary freely. The only constraints in the fitting procedure were that n_{i1} and σ should be ≥ 0. The best fit parameters for the styrene segment distributions are listed in Table 4. A similar situation prevailed at the CMC (Figure 8B), although the greater reflectivity above the background allowed extension of the structure factor to $Q = 0.15$ Å^{-1}, consistent with a larger contribution to the reflectivity due to the greater styrene surface excess (Table 4). Again, an adequate fit was obtained using a single uniform layer model. The data proved insensitive to fitting a double uniform layer model of two nonoverlapping layers.

Styrene self-partial-structure factors at the two highest copolymer concentrations (Figures 8C and 8D) could not be fitted using a single uniform layer model. A double uniform layer model, although producing double-peaked variation of Q^2h_{ii} with Q, could not reproduce the position of both peaks observed in Figures 8C and 8D. A triple uniform distribution was found to fit the data extremely well (eq A7 in the appendix) as shown by the solid lines in the figures. The pictorial representation of this distribution is given in Figure 7 and

Table 4. Parameters Obtained from the Analysis of Styrene Self-Partial-Structure Factors

sample	N^a	layer[b]	$n_S{}^c$ (±), $\times 10^{-4}$ Å^{-3}	width[d] (±), Å	δ (±), Å	$\Gamma_S{}^e$ (±), mg m^{-2}
A	1U	1	3.81 (0.09)	35.9 (1.4)		0.24 (0.01)
B	1U	1	4.91 (0.09)	30.1 (1.1)		0.26 (0.01)
C	3U	1	9.38 (0.26)	23.4 (0.9)		0.38 (0.01)
		2	2.38 (0.41)	31.0 (2.2)	36.7 (0.5)	0.13 (0.01)
		3	3.28 (0.46)	10.7 (2.0)		0.06 (0.01)
D	3U	1	15.46 (0.24)	16.2 (0.6)		0.43 (0.01)
		2	1.36 (0.31)	27.6 (2.6)	34.6 (0.3)	0.07 (0.01)
		3	2.52 (0.35)	9.2 (1.3)		0.04 (0.01)

[a] N is the number of distributions included in the model structure-factor equations (see Appendix): 1U refers to the single uniform distribution of Figure 8A, 3U to the triple uniform distributions (polymer and solvent), and 2UP to the uniform-parabolic EO distribution. [b] The specific layer of each distribution: 1 is the layer closest to the surface and 2 and 3 occur further into the bulk solution, respectively. [c] n_i is the maximum number density of component i. [d] Width is the thickness of the layer. [e] The surface excess quantity for the layer.

Table 5. Parameters Obtained from the Ethylene Oxide Self-PSF Analysis

sample	N^a	layer[b]	$n_{EO}{}^c$ (±), $\times 10^{-3}$ Å^{-3}	width[d] (±), Å	$\Gamma_{EO}{}^e$ (±), mg m^{-2}
A	1U	1	2.29 (0.02)	33.9 (0.5)	0.57 (0.01)
B	2UP	1	2.04 (0.06)	28.0 (0.8)	0.42 (0.01)
		2	0.32 (0.11)	71.3 (6.9)	0.11 (0.01)
C	2UP	1	3.44 (0.08)	30.0 (0.9)	0.75 (0.01)
		2	2.07 (0.16)	108.2 (2.7)	1.09 (0.01)
D	2UP	1	3.80 (0.07)	29.7 (2.0)	0.83 (0.01)
		2	3.15 (0.16)	142.6 (3.0)	2.19 (0.01)

[a] N is the number of distributions included in the model structure-factor equations (see Appendix): 1U refers to the single uniform distribution of Figure 8A, 3U to the triple uniform distributions (polymer and solvent), and 2UP to the uniform-parabolic EO distribution. [b] The specific layer of each distribution: 1 is the layer closest to the surface and 2 and 3 occur further into the bulk solution, respectively. [c] n_i is the maximum number density of component i. [d] Width is the thickness of the layer. [e] The surface excess quantity for the layer.

Table 6. Parameters Obtained from Analysis of Water Self-Partial-Structure Factors

sample	N^a	layer[b]	$n_W{}^c$ (±), $\times 10^{-2}$ Å^{-3}	width[d] (±), Å
A	3U	1	2.34 (0.14)	15.7 (1.8)
		2	3.16 (0.03)	26.9 (4.5)
		3	3.24 (0.02)	31.6 (4.6)
B	3U	1	2.44 (0.07)	19.9 (1.8)
		2	2.99 (0.01)	39.1 (0.7)
		3	3.19 (0.01)	33.8 (1.1)
C	3U	1	2.82 (0.01)	21.3 (0.5)
		2	3.20 (0.02)	45.4 (4.7)
		3	3.24 (0.02)	25.9 (4.4)
D	3U	1	2.34 (0.04)	22.2 (0.6)
		2	2.97 (0.07)	50.0 (1.9)
		3	3.19 (0.05)	37.1 (4.1)

[a] N is the number of distributions included in the model structure-factor equations (see Appendix): 1U refers to the single uniform distribution of Figure 8A, 3U to the triple uniform distributions (polymer and solvent), and 2UP to the uniform-parabolic EO distribution. [b] The specific layer of each distribution: 1 is the layer closest to the surface and 2 and 3 occur further into the bulk solution, respectively. [c] n_i is the maximum number density of component i. [d] Width is the thickness of the layer. [e] The surface excess quantity for the layer.

there are eight parameters needed to describe the distribution: three number densities (n_{i1}, n_{i2}, and n_{i3}), three widths (σ, ϵ, and τ), and two separation distances (δ_1 and δ_2). Initially, fits were obtained by allowing each parameter to vary freely (subject to all parameters ≥ 0 and no overlap of distributions), but it was established that δ_1 and δ_2 were equal within the uncertainties. The lines presented in Figures 8C and 8D therefore correspond to fits obtained by constraining $\delta_1 = \delta_2$. From the fitted parameters given in Table 4, n_{i3} is greater than n_{i2} for both concentrations studied. The individual surface excess (in mg m^{-2}) of each layer of styrene at the interface is also given in Table 4 and was calculated using eqs A5 or A8.

Ethylene Oxide Self-Partial-Structure Factors. Figure 9 shows the self-PSFs obtained for the ethylene oxide (EO) segments. The partial structure factors at all concentrations were initially fitted using the uniform-parabolic layer model, the structure factor for which is given by eq A10 (all parameters being allowed to vary freely for values greater than or equal to zero). The data for the lowest concentration (Figure 9A) proved insensitive to the parabolic part of the distribution; this structure factor was therefore fitted using the single uniform layer model and this is displayed in Figure 10A. The parameters obtained by this fitting to the EO segment distributions are given in Table 5. For the two lowest concentrations investigated the fits are good, the useful Q-range of data again being dictated by the background subtraction. The fits (uniform layer plus parabolic profile model) to the data of the two highest concentrations (Figures 9C and 9D) are satisfactory over the available Q-range, but there are some discrepancies. Such discrepancies are not surprising considering the idealized nature of the uniform-parabolic profile. It should be noted that the other idealized distributions used to fit the EO structure factors (e.g., multiple uniform layers or a Gaussian distribution) displayed qualitatively similar discrepancies but larger χ^2 values, implying poorer fits overall. No account has been made for the slight differences in concentration of the solutions used for each contrast condition (<1% variation) and small differences in the individual copolymer compositions. Considering these factors, the quality of the fits obtained are good. The associated surface excess quantities obtained from eq A11 are given in Table 5.

Water Self-Partial-Structure Factors. Water self-partial-structure factors were fitted (Figure 10) using the triple uniform layer model and the parameters are listed in Table 6. A single uniform distribution was unable to fit any of the near-surface water layer self-partial-structure factors at all. Disagreement between data and model is most apparent in the range $0 < Q/\text{Å}^{-1} < 0.04$, the region associated with greater depth scales normal to the surface. The best agreement obtained between the data and model is that for the lowest copolymer concentration (Figure 10A). As can be seen in Figures 10B and 10D, the data fall below the model curves at lower Q-values, and although this is not so

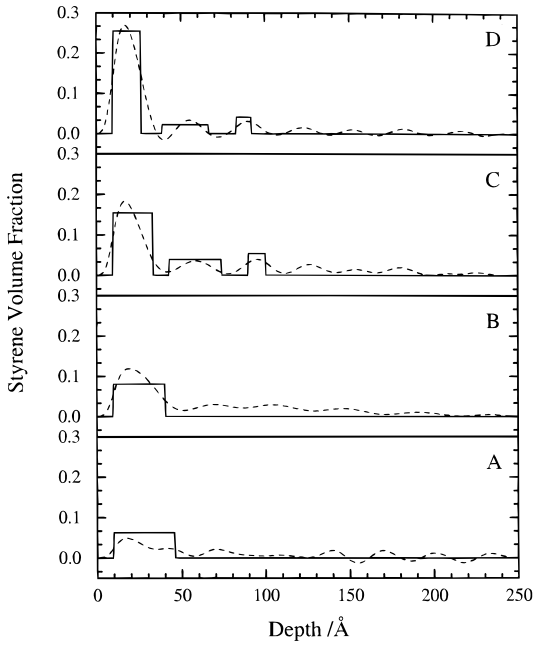

Figure 11. Comparison of styrene volume fraction profiles calculated from model independent analysis (- - -) and the partial-structure factor analysis (—) for all four concentrations.

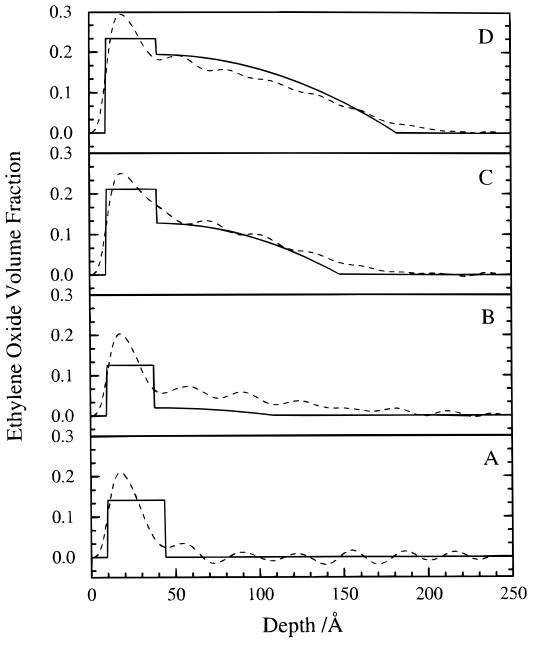

Figure 12. Comparison of ethylene oxide volume fraction profiles calculated from the model independent analysis (- - -) and partial-structure factor analysis (—) for each concentration.

evident in Figure 10C, it is still nevertheless apparent. Similar behavior in water self-partial-structure factors for other EO-containing systems at the air−water interface have been reported earlier.[40] Such anomalous behavior is not due to the shortcomings of the kinematic approximation because the reflectivities do not approach values where this approximation breaks down. This behavior of water self-partial-structure factors has been observed in relatively low molecular weight EO-containing systems (nonionic surfactants) at sufficiently high concentrations of EO. The cause of this behavior has yet to be identified.

Cross Partial-Structure Factors. The cross partial-structure factor is defined generally as

$$Q^2 h_{ij}(Q) = Q^2 |\hat{n}_i(Q)\hat{n}_j^*(Q)| \qquad (8)$$

in which i and j represent different components. Due to the complicated nature of eqs A6, A9, and A12 the cross partial-structure factor equations have not been calculated. No information regarding the relative separation between the component distributions has therefore been gained from partial-structure factor analysis. This is not a problem since the relevant separations are clearly evident in the MI-determined volume fraction profiles of Figure 7.

Discussion

The volume fraction profiles calculated for each component via the MI and PSF analysis methods are compared in Figures 11−13. The two methods give remarkably similar results in the 50-Å region closest to the solution surface. The value of $z = 0$ is placed arbitrarily at the point where the MI-obtained solvent number density is zero. The overall picture obtained is that the majority of S segments are situated in a region that begins at the interface and extends below it (Figure 11), the penetration depth depending on the copolymer concentration. This region also contains a substantial amount of the EO segments (Figure 12).

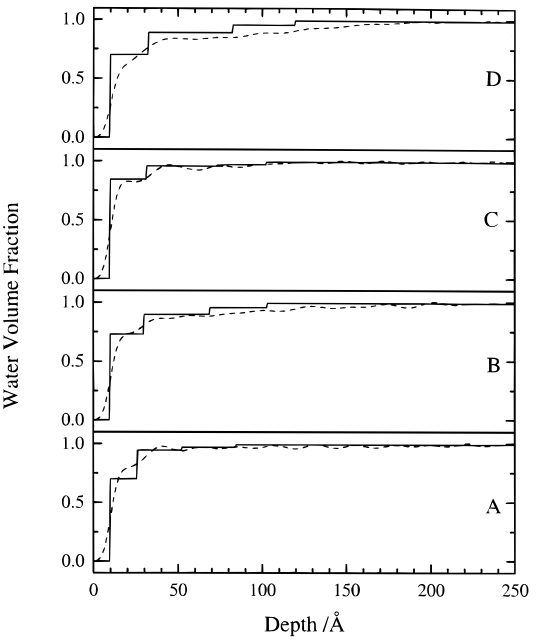

Figure 13. Comparison of water volume fraction profiles obtained from the model independent analysis (- - -) and partial-structure factor analysis (—).

Figure 13 shows a significant depletion of water in this same region. The maxima in ϕ_S and ϕ_E in the near-surface region increase with an increasing bulk concentration of the copolymer as expected for surfactant behavior. The observation of S segments below the solution surface is counterintuitive since these would be expected to lie almost exclusively in the air phase. A significant number of EO segments are also in the same region immediately below the surface, suggesting that the hydrophilic EO segments form a protective shell around the hydrophobic S segments; this is consistent with surface micellization. Note that the thickness of the first styrene layer below the surface decreases

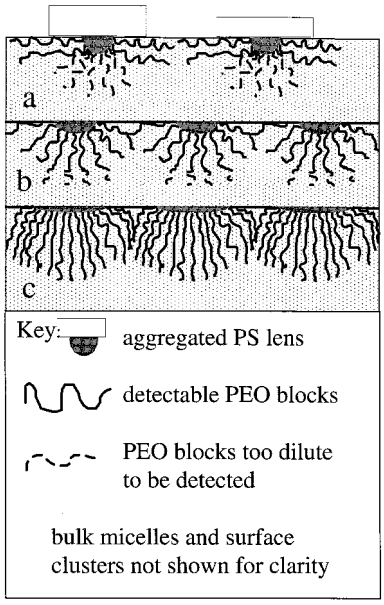

Figure 14. Schematic representation of the change in surface micelle organization with increasing copolymer concentration (a−c). As the bulk concentration increases, the PS lenses thin and spread across the solution surface and the PEO chains desorb and extend into solution. At the highest concentration studied (10^{-3} g mL^{-1}, Figure 15c) the PEO chains are extended and form a brushlike organization.

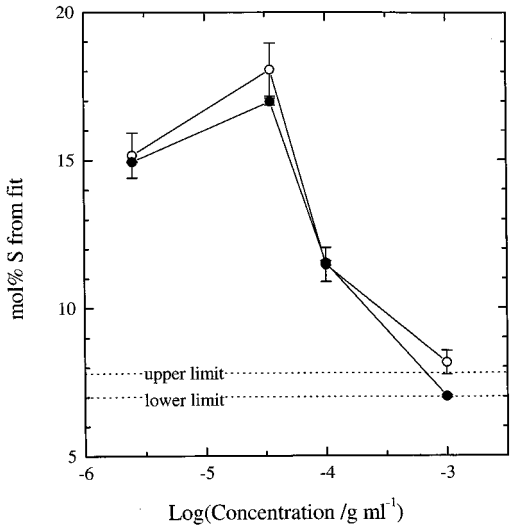

Figure 15. Mole percent styrene segments in the copolymer determined from the neutron reflectometry data: (○) model independent analysis; (●) partial-structure factor analysis. The upper and lower limits indicate the expected composition range from the copolymer analysis data of Table 2.

significantly as Γ_S increases, whereas the EO uniform layer thickness remains approximately constant across the entire concentration range studied. The picture that emerges is one of surface micelles consisting of many copolymer molecules forming hemispherical surface structures where the PS, being hydrophobic, attempts to maximize its contact with air and minimize its contact with water. Thus, at low surface excess the PS in each surface micelle forms structures reminiscent of oil-on-water lenses. The PS lenses only partially wet the solution surface as depicted in Figure 14a. The mean thickness of this layer of PS, as determined from the NR data in Table 4 (sample A), is very close to the 33 Å expected for a fully extended all-trans PS chain of 12 repeat units with a *sec*-butyl end group, and assuming an effective C−C bond length of 1.27 Å.[41] Around the curved interfaces of the PS lenses are the chemically grafted PEO chains which form the partial corona of the surface micelle. PEO is in itself surface-active due to the amphiphillic nature of the EO units and so the PEO chains are, at least in part, adsorbed weakly to the air−water interfacial areas between the PS lenses.

As the bulk concentration of the copolymer increases, the PS lenses thin and in order to obtain the observed increase in Γ_S, they must spread across the air−water interface (Figure 15b) (i.e., the PS lenses wet the surface more effectively). Consequently, reducing the surface area available to the weakly adsorbing PEO chains forces them to desorb and extend deeper into the solution. This extension becomes apparent near the bulk CMC value as shown by the development of the PEO tail in Figure 13B. The spreading and thinning of the PS lenses continue to the highest concentration studied, as does the extension of the PEO chains into solution.

Although our data imply that the association of the PS−PEO copolymer occurs at the surface, because the barrier for direct adsorption of micelles to a wall is extremely high,[16] unassociated copolymers are initially adsorbed to the surface. PS blocks then associate at the surface into the energetically favorable morphology of droplets. Ligoure[22] has shown theoretically that, for an AB copolymer in a selective solvent for the B block adsorbing onto a solid wall, the formation of droplets of the A blocks (surface micelles) occurs at a bulk concentration that is different from the CMC. This concentration was termed the critical surface micelle concentration (CSMC), and the surface micelles remain in equilibrium with free unimers in bulk and at the surface. Our data supports Ligoure's theoretical prediction because surface micellization occurs at 2.5×10^{-6} g mL^{-1}, an order of magnitude smaller than the observed bulk CMC of 3.5×10^{-5} g mL^{-1}. Surface micellization has also been cited[42] as the source of discontinuities in surface pressure isotherms of spread surfactants and phospholipids. Although surface micelles have been observed in spread and deposited films of other diblock copolymers[9,10,43−46] and predicted by others,[47] this appears to be the first report for its occurrence in a surface excess layer of a diblock copolymer without any ionic groups. The "plateau" observed in Figure 3 resembles the non-first-order phase transitions seen in spread films of diblock copolymers since it occurs over varying γ_0 and is indicative of surface micellization of the adsorbing PS−PEO copolymer.

Only a single PS layer at the interface is evident at the CMC and lower concentrations of the copolymer. The appearance of second and third discrete styrene layers is clearly evident in the volume fraction profiles of Figures 11C and 11D. The layered PS structure occurs at a bulk concentration of 10^{-4} g mL^{-1} that is coincident with the kink in the γ_0 variation (Figure 3). Block copolymers in the solid state have a microphase-separated morphology, determined by the copolymer composition.[48−50] The presence of a selective solvent in an AB copolymer simply increases the apparent volume of the soluble B blocks and in the solvent-swollen state AB copolymers display more than one kind of mesoscopic structure.[51] For lamellar structures which occur when $\phi_A \approx \phi_B$, the interface between segregated domains is planar since this represents the most spatially

favorable way of packing immiscible, end-tethered blocks of equal volume fractions. By the same argument the spherical and cylindrical structures are the most efficient way of packing immiscible blocks when $\phi_A < \phi_B$ since the space available on the convex side of the interface (containing B) is larger than the space on the concave side (containing A). Of the two, spherical structures offer the most volume to the B block and so are the most commonly observed structures when $\phi_A \ll \phi_B$. Since the layered PS organization at the air−water interface of the PS−PEO copolymer is observed with no accompanying discrete layering of the PEO blocks, the layering observed is not due to a transition at the solution surface to a lamellar-type structure. The layering of PS blocks in the same region as a continuous PEO/solvent matrix can only be rationalized by spherical or cylindrical PS domains surrounded by the PEO/water matrix. The reflectivity data do not allow us to distinguish between PS spheres or cylinders, however, because the volume fraction profiles represent the average structure as a function of distance through the interface. The regular spacing between the centers of the PS layers ($\delta \approx 35$ Å from Table 4) could perhaps be indicative of ordering of spherical micelles at the surface into a cubic-type lattice, or cylindrical micelles into hexagonal arrays. Such ordered systems are often observed in surfactant solutions. Therefore, the phase transition observed in the surface tension data may be due to a disorder−order transition. The disordered state being one in which micelles are randomly distributed in the surface excess region and the ordered state intervenes at higher surface concentrations to reduce interaction between micelles, reducing the overall free energy. Clustering of PS−PEO micelles in bulk solutions has been observed.[2−4,8] In the dry state the volume fraction of styrene in the copolymer is 0.18 ± 0.01. In the strong segregation limit and for amorphous EO blocks, this volume fraction would probably result in cylindrical domains in a PEO matrix. In the situation reported here the surface region is highly solvated and so $\phi_S \ll 0.18$; therefore, the layer-like organization of PS in the surface region is most probably due to clustering of spherical micelles.

Although ϕ_S will be clearly much less than 0.18 in the highly solvated surface region, it is difficult to calculate an exact value. This is because the NR technique is not sensitive to all segments at the surface. This is seen clearly in Figure 15 where the mol % of S obtained from the NR fits has been plotted versus log(concentration). From the copolymer characterization it was calculated that the mol % of S in the dry copolymer was 7.4 ± 0.4. In the solution this value should still hold when the solvent fraction is ignored. The data in Figure 15, however, show that at almost all concentrations studied there appears to be a higher relative amount of PS. The apparent mol % of S values in the figure have been calculated via

$$\frac{\Gamma_S^0/m_S \times 100\%}{\Gamma_S^0/m_S + \Gamma_{EO}^0/m_{EO}} \qquad (9)$$

where Γ_i^0 is the total surface excess of component i at the surface (mg m^{-2}) and m_i is the molar mass of segment i. The apparent Γ_i^0 values are also listed in Table 7 for the S and EO segments, along with the calculated apparent mol % of S from eq 9. The values in the MIF column subheadings were calculated by numerical integration of the area under the relevant number density profiles and appear as the open circles in Figure 15. The values listed under PSF subheadings were calculated from the appropriate expressions A5, A8, and A11 given in the Appendix and are represented by the closed circles in Figure 15. The uncertainty in the integration of the MIF values is estimated to be 5%, and this is the origin of the error bars in Figure 15. The agreement between the mol % S values calculated from MIF and PSF analyses is good; hence, the deviations from the experimental value of 7.4 ± 0.4 are real. Only at the highest concentration studied do the apparent values agree with the expected value within their associated uncertainties (the upper and lower limits of the expected value are labeled as such in Figure 15). We associate the discrepancy at lower concentrations as being due to dilute EO segments not being detectable by the NR technique, presumably because the reflectivity of dilute EO segments has a magnitude less than or equal to the background. Similar effects have been observed for PEO homopolymer surface excess layers.[52]

Table 7. Surface Excess Concentrations from Analysis of NR Data by MI and PSF Methods and the Copolymer Composition Resulting from These Compositions

	Γ_S^0/mg m^{-2}		Γ_{EO}^0/mg m^{-2}		mol % S	
sample	MI	PSF	MI	PSF	MI	PSF
A	0.24	0.24	0.58	0.57	15.2	14.9
B	0.62	0.26	1.19	0.53	18.1	17.0
C	0.65	0.57	2.11	1.84	11.5	11.5
D	0.61	0.54	2.92	3.01	8.2	7.0

Spread films of PS−PEO diblock copolymers have been investigated by Goncalves da Silva et al.[13] and their analysis of the surface pressure isotherms provides support for surface micellization. At low surface concentrations the copolymer has a surface organization of overlapping pancakes which transforms to a quasi-brush-like layer with PEO extending into the subphase when the surface tension reaches ~62.5 mN m^{-1}. For a PEO block of similar molecular weight to that used by us, the limiting area per segment in this pancake region corresponds to a PEO surface excess of 0.27 mg m^{-2}. This is approximately twice the value predicted by the Alexander brush model[54] where brush formation would take place (this transition is when the molecular area at the interface is $\sim R_g^2$ and $R_g \sim aN^{3/4}$, with the statistical step length of PEO being 4.5 Å[55]). There was no suggestion by Goncalves da Silva et al. that surface micellization could be taking place, although a non-first-order phase transition in surface tension was observed, such a phase transition also being observed by Bijsterbosch et al.[12] In both these cases the surface excess of the PEO was approximately twice of that anticipated for homopoly(ethylene oxide) to form a brush-like layer according to the Alexander model. Surface excesses of PEO calculated from our NR data are given in Table 7 and these are approximately 4 times the Alexander model prediction. In Table 8 we report the surface excess layer concentration of the copolymer calculated directly from the neutron reflectivity data and using the known styrene content to correct for any underestimation of PEO present due to the dilution of segments distant from the interface. These values indicate a huge excess of PEO in the surface excess region, and one way of accommodating the PEO is by locating it at a curved interface, thus reducing or eliminating spatial restrictions. As the surface concentration increases, the polystyrene micelle cores flatten against the air−water

Table 8. Copolymer Surface Excess from NR Data

	$\Gamma_{PS-PEO}{}^{0\,a}$/mg m^{-2}		$\Gamma_{PS-PEO}{}^{0\,b}$/mg m^{-2}	
sample	MI	PSF	MI	PSF
A	0.82	0.80	1.55	1.49
B	1.81	0.78	3.93	1.62
C	2.76	2.41	4.10	3.60
D	3.54	3.55	3.89	3.41

[a] Calculated from values of Table 7. [b] Calculated assuming 7.4 mol % S.

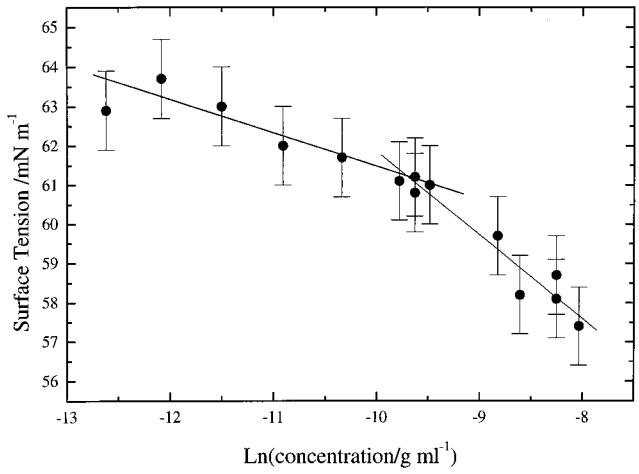

Figure 16. Surface tension data as a function of the natural logarithm of the bulk concentration of diblock copolymer. The lines are least-squares fit to the two groups of data.

interface and the PEO blocks have to stretch deeper into the subphase to relieve excluded volume effects. This stretching is clearly evident in Figures 12C and 12D. We have also attempted to obtain the surface excess concentration of the copolymer from the variation of surface tension with concentration. These data form two linear groups when plotted as a function of Ln(c) in Figure 16. Application of the Gibbs adsorption isotherm to each of these gives a surface excess of approximately 3.5 mg m^{-2} when the bulk dispersion concentration is less than 1×10^{-4}g mL. this value is in fair agreement with that obtained from the neutron reflectivity data. For bulk dispersion concentrations greater than this, the slope of the surface tension as a function of Ln(c) gives a surface excess of approximately 12.8 mg m^{-2} far greater than that provided by the neutron reflectometry data. It is noteworthy that at this bulk concentration (and above) of copolymer we observe a "layering" of the polystyrene volume fraction in the near-surface region which is accompanied by the development of a parabolic tail for the poly(ethylene oxide) component. The applicability of the Gibbs adsorption isotherm in these circumstances is questionable and the surface excess value obtained is most probably an artifact.

We now turn to discuss whether surface micelles would be expected to be present at the lowest concentration studied in this work. Bulk micelles begin to form at approximately 3.5×10^{-5} g mL^{-1} and are completely formed at 10^{-4} g mL^{-1}. The spontaneous adsorption of the copolymer to the air−water surface dictates that there will always be a higher PS−PEO concentration at the surface relative to that in the bulk dispersion. Based on this simple fact it is clear that micelles should begin to form at the surface at a bulk concentration that is less than the CMC. Assuming naively that the surface-region micelles begin to form at a local concentration that is equivalent to the bulk CMC value, we can provide an estimate of the styrene repeat unit number density at which surface micelles will be present. The bulk CMC value equates to a styrene segment number density, n_S, of 3.23×10^{-8} Å^{-3}. At the lowest concentration studied the value of n_S fitted to the NR data using the uniform layer model was $(3.81 \pm 0.09) \times 10^{-4}$ Å^{-3} (Table 4) which is the concentration of S segments in the layer just below surface. Since the fitted value is 4 orders of magnitude greater than the bulk CMC value, it is clear that surface micelles should be present at every concentration studied by us.

Conclusions

Static light scattering from aqueous solutions of PS−PEO copolymers has shown that the copolymers aggregate spontaneously into micelles with the CMC occurring at approximately 3.5×10^{-5} g mL^{-1} at 298 K. The micelles have an asymptotic hydrodynamic radius indicative of the closed association regime, at 10^{-4} g mL^{-1}. The copolymer is surface-active and forms an adsorbed layer at the air−solution interface. Surface tensions as a function of bulk concentration show that there is a non-first-order phase transition occurring at the surface between the concentrations of 3.5×10^{-5} and 10^{-4} g mL^{-1}. NR experiments exploring the range of contrast variation available have provided insights into the surface organizational behavior of PS−PEO copolymers at these two concentrations. Two further concentrations were also studied, one well-below the CMC (2.5×10^{-6} g mL^{-1}) and one well-above (10^{-3} g mL^{-1}). From the NR data the behavior of the copolymers at the air−solution interface was found to display many parallels with that of the copolymer in bulk dispersion. In particular, the adsorbed copolymers form micelles at the surface as they do in bulk. Bulk micelles are composed of an inner core of PS surrounded by a corona of extended PEO chains. The same salient features are observed for the surface micelles. Similar surface micelles have been observed for insoluble spread and deposited copolymer monolayers, but this report is the first recorded case of soluble copolymers with no ionic groups also displaying surface phase separation behavior. Well-below the CMC the PS−PEO surface micelles exist in which both PS and PEO chains are adsorbed to the air−solution surface. The PS cores form lenses at the surface which initially have a high curvature. As the bulk concentration is raised toward the CMC, the adsorbed amount increases, the number of PS lenses at the surface grow, and the lenses spread (i.e., a higher density PS layer results with a reduced average layer thickness). The increased coverage of the surface with PS forces PEO chains to extend deeper into the subphase. These extended PEO chains are of a sufficiently high concentration near the PS lens to be detectable by NR. The ends of the PEO chains, however, are apparently too dilute to be detectable. As the bulk concentration increases well-above the CMC, the PS lenses cover the air−solution interface more effectively and their curvature decreases further. The already partially extended PEO chains stretch further into solution, becoming more concentrated and hence detectable to greater distances from the air−water interface, and at a bulk concentration of approximately 10^{-3} g mL^{-1} the PEO chains form an extended brush-like layer grafted to the PS lens interfaces. The height of the interfacial brush is 5% larger than R_h as expected

from theory. Clustering of micelles into larger surface aggregates is observed at bulk concentrations of 10^{-4} g mL^{-1} or greater, this being the cause of the non-first-order phase transition observed in the γ_0 versus bulk concentration plot.

Acknowledgment. We thank the EPSRC for the financial support of the research program of which this work forms part. The authors also thank F. T. Kiff for the copolymer synthesis and purification, G. M. Forrest for SEC characterization, and J. M. Say for NMR characterization. M.R.L. thanks G. J. Bown and A. S. Brown for assistance with the NR experiments.

Appendix

Derivation of Model-Partial Structure Factors. *(A) Single Uniform Polymer Segment Distribution.* The number-density profile of polymer segment i in a single uniform distribution is defined as

$$n_i(z) = n_{i1} \qquad -\sigma/2 < z < \sigma/2$$
$$= 0 \qquad \text{for all other } z$$

where σ is the layer thickness (Å) and n_{i1} the maximum segment number density ($Å^{-3}$). The Fourier transformed number density $\hat{n}_i(Q)$ is obtained through

$$\hat{n}_i(Q) = \int_{-\sigma/2}^{\sigma/2} n_{i1} \exp(-\mathbf{i}Qz)\, dz \qquad \text{(A1)}$$

the result of which is

$$\hat{n}_i(Q) = \frac{2n_{i1}}{Q} \sin\left(\frac{Q\sigma}{2}\right) \qquad (Å^{-2}) \qquad \text{(A2)}$$

The self-partial-structure factor $h_{ii}(Q)$ is defined generally as

$$h_{ii}(Q) = |\hat{n}_i(Q)|^2 \qquad \text{(A3)}$$

which, upon rearrangement, yields the expression in the form used in this paper:

$$Q^2 h_{ii}(Q) = 4{n_{i1}}^2 \sin^2\left(\frac{Q\sigma}{2}\right) \qquad (Å^{-6}) \qquad \text{(A4)}$$

The associated surface excess quantity of component i, Γ_i, is defined simply as

$$\Gamma_i = n_{i1}\sigma \qquad (Å^{-2}) \qquad \text{(A5)}$$

(B) Triple Uniform Polymer Segment Distribution. The number-density profile defined above is simply extended to be comprised of three uniform layers. Thus, the Fourier transformation of the density profile is defined as

$$\hat{n}_i(Q) = \frac{2n_{i1}}{Q} \sin\left(\frac{Q\sigma}{2}\right) + \frac{\mathbf{i}n_{i2}}{Q}\left[\exp\left(\mathbf{i}Q\left(\delta_1 - \frac{\epsilon}{2}\right)\right) - \exp\left(\mathbf{i}Q\left(\delta_1 + \frac{\epsilon}{2}\right)\right)\right] + \frac{\mathbf{i}n_{i3}}{Q}\left[\exp\left(\mathbf{i}Q\left(\delta_2 + \delta_1 - \frac{\tau}{2}\right)\right) - \exp\left(\mathbf{i}Q\left(\delta_2 + \delta_1 + \frac{\tau}{2}\right)\right)\right] \qquad \text{(A6)}$$

which results in a self-partial-structure factor of

$$Q^2 h_{ii}(Q) = 4{n_{i3}}^2 \sin^2\left(\frac{Q\tau}{2}\right) + 4{n_{i2}}^2 \sin^2\left(\frac{Q\epsilon}{2}\right) + 4{n_{i1}}^2 \sin^2\left(\frac{Q\sigma}{2}\right) + 8n_{i2} \sin\left(\frac{Q\epsilon}{2}\right)\left[n_{i3} \sin\left(\frac{Q\tau}{2}\right)\cos(Q\delta_2) + n_{i1} \sin\left(\frac{Q\sigma}{2}\right)\cos(Q\delta_1)\right] + 8n_{i1}n_{i3} \sin\left(\frac{Q\tau}{2}\right)\sin\left(\frac{Q\sigma}{2}\right)\cos(Q(\delta_1 + \delta_2)) \qquad \text{(A7)}$$

The total surface excess of polymer segment i is calculated by summing over the individual layer surface excesses:

$$\Gamma_i = n_{i1}\sigma + n_{i2}\epsilon + n_{i3}\tau \qquad \text{(A8)}$$

Equations A6−A8 can be reduced to that for a double uniform polymer segment distribution by substituting zero for n_{i3}. Further substitution of zero for n_{i2} yields the single uniform polymer segment distributions of section A above. Another useful simplification that may be valid for some distributions could be to have non-separated uniform layers. This is achieved mathematically by substituting $\sigma/2 + \epsilon/2$ for δ_1 and $\epsilon/2 + \tau/2$ for δ_2.

(C) Uniform-Parabolic Polymer Segment Distribution. The number-density profile is defined generally as

$$n_i(z) = 0 \qquad z < -\sigma/2$$
$$= n_{i1} \qquad -\sigma/2 < z < \sigma/2$$
$$= n_{i2}\left(1 - \frac{(z - \sigma/2)^2}{\epsilon^2}\right) \qquad \sigma/2 < z < \epsilon + \sigma/2$$
$$= 0 \qquad z > \epsilon + \sigma/2$$

from which $\hat{n}_i(Q)$ becomes

$$\hat{n}_i(Q) = \frac{\mathbf{i}n_{i1}}{Q} - \frac{\mathbf{i}n_{i1}}{Q}\exp(\mathbf{i}Q\sigma) + \frac{\mathbf{i}n_{i2}}{Q^3{\epsilon^2}}(2 + Q^2\epsilon^2)\exp(\mathbf{i}Q\sigma) - \frac{2\mathbf{i}n_{i2}}{Q^3{\epsilon^2}}\exp(\mathbf{i}Q(\sigma + \epsilon)) - \frac{2n_{i2}}{Q^2\epsilon}\exp(\mathbf{i}Q(\sigma + \epsilon)) \qquad \text{(A9)}$$

The partial-structure factor is therefore

$$Q^2 h_{ii}(Q) = 2{n_{i1}}^2 + {n_{i2}}^2 - 2n_{i1}n_{i2}\cos(Q\sigma)[n_{i2} - n_{i1}] + \frac{1}{Q^4{\epsilon^4}}\left\{\begin{array}{l} 8{n_{i2}}^2[1 + Q^2\epsilon^2] \\ + [\cos(Q\epsilon) + Q\epsilon \sin(Q\epsilon)][4n_{i1}n_{i2}Q^2\epsilon^2 - 4{n_{i2}}^2Q^2\epsilon^2 - 8{n_{i2}}^2] \\ + 4n_{i1}n_{i2}Q^2\epsilon^2[\cos(Q\sigma) - \cos(Q(\sigma + \epsilon)) - Q\epsilon \sin(Q(\sigma + \epsilon)) - 1] \end{array}\right\} \qquad \text{(A10)}$$

and the surface excess can be found from

$$\Gamma_i = n_{i1}\sigma + \frac{2}{3}n_{i2}\epsilon \qquad \text{(A11)}$$

Equations A9−A11 can be reduced to the equivalent of a parabolic decay profile (i.e., with no uniform distribution) by substituting zero for n_{i1}. Such a polymer segment distribution could be employed to analyze reflectivity data from densely end-grafted polymers forming brushes of the type described by Milner et al.[57]

(D) Triple Uniform Solvent Distribution. The solvent number density profile $n_W(z)$ is defined as

$$\begin{aligned} n_W(z) &= 0 && z < -\sigma/2 \\ &= n_{W1} && -\sigma/2 < z < \sigma/2 \\ &= n_{W2} && \sigma/2 < z < \epsilon + \sigma/2 \\ &= n_{W3} && \epsilon + \sigma/2 < z < \tau + \epsilon + \sigma/2 \\ &= n_{W0} && z > \tau + \epsilon + \sigma/2 \end{aligned}$$

where n_{W0} is the bulk number density of water. This leads to $\hat{n}_W(Q)$ as being

$$\hat{n}_W(Q) = \frac{2n_{W1}}{Q}\sin\left(\frac{Q\sigma}{2}\right) + \frac{\mathbf{i}n_{W2}}{Q}\left[\exp\left(-\mathbf{i}Q\left(\epsilon + \frac{\sigma}{2}\right)\right) - \exp\left(-\frac{\mathbf{i}Q\sigma}{2}\right)\right] + \frac{\mathbf{i}n_{W3}}{Q}\left[\exp\left(-\mathbf{i}Q\left(\tau + \epsilon + \frac{\sigma}{2}\right)\right) - \exp\left(-\mathbf{i}Q\left(\epsilon + \frac{\sigma}{2}\right)\right)\right] - \frac{\mathbf{i}n_{W0}}{Q}\exp\left(-\mathbf{i}Q\left(\tau + \epsilon + \frac{\sigma}{2}\right)\right) \quad \text{(A12)}$$

and the self-partial-structure factor as

$$Q^2 h_{WW}(Q) = {n_{W1}}^2 + (n_{W1} - n_{W2})^2 + (n_{W2} - n_{W3})^2 + (n_{W3} - n_{W0})^2 + 2n_{W1}(n_{W2} - n_{W1})\cos(Q\sigma) + 2(n_{W1} - n_{W2})(n_{W3} - n_{W3})\cos(Q\epsilon) + 2(n_{W2} - n_{W3})(n_{W3} - n_{W0})\cos(Q\tau) + 2n_{W1}(n_{W3} - n_{W2})\cos(Q(\epsilon + \sigma)) + 2(n_{W3} - n_{W0})(n_{W1} - n_{W2})\cos(Q(\tau + \epsilon)) + 2n_{W1}(n_{W0} - n_{W3})\cos(Q(\tau + \epsilon + \sigma)) \quad \text{(A13)}$$

Equations A12 and A13 can be reduced to the equivalent of a double uniform solvent distribution by substituting zero for τ and n_{W0} for n_{W3}. The equations can be further reduced to a single uniform distribution by substituting zero for ϵ and n_{W0} for n_{W2}.

References and Notes

(1) Nakamura, K.; Endo, R.; Takeda, M. *J. Polym. Sci., Polym. Phys. Ed.* **1976**, *14*, 135.
(2) Xu, R.; Winnik, M. A.; Hallett, F. R.; Riess, G.; Croucher, M. D. *Macromolecules* **1991**, *24*, 87.
(3) Wilhelm, M.; Zhao, C.-L.; Wang, Y.; Xu, R.; Winnik, M. A.; Mura, J.-L.; Riess, G.; Croucher, M. D. *Macromolecules* **1991**, *24*, 1033.
(4) Xu, R.; Winnik, M. A.; Riess, G.; Chu, B.; Croucher, M. D. *Macromolecules* **1992**, *25*, 644.
(5) Hruska, Z.; Piton, M.; Yekta, A.; Duhamel, J.; Winnik, M. A.; Riess, G.; Croucher, M. D. *Macromolecules* **1993**, *26*, 1825.
(6) Hickl, P.; Ballauff, M.; Jada, A. *Macromolecules* **1996**, *29*, 4006.
(7) Jada, A.; Hurtrez, G.; Siffert, B.; Riess, G. *Macromol. Chem. Phys.* **1996**, *197*, 3697.
(8) Mortensen, K.; Brown, W.; Almdal, K.; Alami, E.; Jada, A. *Langmuir* **1997**, *13*, 3635.
(9) Clarke, C. J.; Lennox, R. B.; Eisenberg, A.; Rafailovich, M. H.; Sokolov, J. In *Solvents and Self-Organisation of Polymers*; Webber, S. E., Munk, P., Tuzar, Z., Eds.; Kluwer Academic Publishers: The Netherlands, 1996; pp 73−81.
(10) Clarke, C. J.; Zhang, L.; Zhu, J.; Yu, K.; Lennox, R. B.; Eisenberg, A. *Macromol. Symp.* **1997**, *118*, 647.
(11) Ikada, Y.; Iwata, H.; Nagaoka, S.; Horii, F.; Hatada, M. *J. Macrmol. Sci., Phys. B* **1980**, *17*, 191.
(12) Bijsterbosch, H. D.; de Haan, V. O.; de Graff, A. W.; Mellema, M.; Leermakers, F. A. M.; Cohen Stuart, M. A.; van Well, A. A. *Langmuir* **1995**, *11*, 4467.
(13) Gonçalves da Silva, A. M.; Filipe, E. J. M.; d'Oliviera, J. M. R.; Martinho, J. M. G. *Langmuir* **1996**, *12*, 6547.
(14) Marques, C.; Joanny, J. F.; Leibler. L. *Macromolecules* **1988**, *21*, 1051.
(15) Satija, S. K.; Majkrzak, C. F.; Russell, T. P.; Sinha, S. K.; Sirota, E. B.; Hughes, G. J. *Macromolecules* **1990**, *23*, 3860.
(16) Johner, A.; Joanny, J. F. *Macromolecules* **1990**, *23*, 5299.
(17) Cosgrove, T.; Heath, T. G.; Phipps, J. S.; Richardson, R. M. *Macromolecules* **1991**, *24*, 94.
(18) Leermakers, F. A. M.; Gast, A. P. *Macromolecules* **1991**, *24*, 718.
(19) Parsonage, E.; Tirrell, M.; Watanabe, H.; Nuzzo, R. G. *Macromolecules* **1991**, *24*, 1987.
(20) Huguenard, C.; Varoqui, R.; Pefferkorn, E. *Macromolecules* **1991**, *24*, 2226.
(21) Tsai. W. H.; Boerio, F. J.; Clarson, S. J.; Parsonage, E. E.; Tirrell, M. *Macromolecules* **1991**, *24*, 2538.
(22) Ligoure, C. *Macromolecules* **1991**, *24*, 2968.
(23) Field, J. B.; Toprakcioglu, C.; Ball, R. C.; Stanley, H. B.; Dai, L.; Barford, W.; Penfold, J.; Smith, G.; Hamilton, W. *Macromolecules* **1992**, *25*, 434.
(24) Nakamura, K.; Endo, R.; Takeda, M. *J. Polym. Sci., Polym. Phys. Ed.* **1976**, *14*, 1287.
(25) Huang, Q. R.; Wang, C. H. *Langmuir* **1996**, *12*, 2679.
(26) Born, M.; Wolf, E. In *Principles of Optics*, 5th ed.; Pergammon Press: Oxford, 1975; p 51.
(27) Abélès, F. *Ann. Phys.* **1948**, *12*, 34.
(28) Hamley, I. W.; Pedersen, J. S. *J. Appl. Crystallogr.* **1994**, *27*, 29.
(29) Crowley, T. L.; Lee, E. M.; Simister, E. A.; Thomas, R. K.; Penfold, J.; Rennie, A. R. *Colloids Surf.* **1990**, *52*, 85.
(30) Anders, H. *Thin Films in Optics*; Focal Press: London, 1967.
(31) Pedersen, J. S. *J. Appl. Crystallogr.* **1992**, *25*, 129.
(32) Pedersen, J. S.; Hamley I. W. *Physica B* **1994**, *198*, 16.
(33) Crowley, T. L.; Lee, E. M.; Simister, E. A.; Thomas, R. K. *Physica B* **1991**, *173*, 143.
(34) Simister, E. A.; Lee, E. M.; Thomas, R. K.; Penfold, J. *J. Phys. Chem.* **1992**, *96*, 1373.
(35) Lyttle, D. J.; Lu, J. R.; Su, T. J.; Thomas, R. K.; Penfold, J. *Langmuir* **1995**, *11*, 1001.
(36) Crowley, T. L. *Physica A* **1993**, *195*, 354.
(37) Jialanella, C. L.; Firer, E. M.; Piirma, I. *J. Polym. Sci., Part A: Polym. Chem.* **1992**, *30*, 1925.
(38) Hunter, R. J. *Foundations of Colloid Science, Vol. I*; Oxford University Press: Oxford, 1987.
(39) Richards, R. W.; Rochford, B. R.; Webster, J. R. P. *Faraday Discuss.* **1994**, *98*, 263.
(40) Ariga, K.; Okahata, Y. *Langmuir* **1994**, *10*, 3255.
(41) Israelachvili, J. *Langmuir* **1994**, *10*, 3774.
(42) Zhu, J.; Lennox, R. B.; Eisenberg, A. *Langmuir* **1991**, *7*, 1579.
(43) Zhu, J.; Lennox, R. B.; Eisenberg, A. *J. Phys. Chem.* **1992**, *96*, 4727.
(44) Li, S.; Hanley, S.; Khan, I.; Varshney, S. K.; Eisenberg, A.; Lennox, R. B. *Langmuir* **1993**, *9*, 2243.
(45) Li, Z.; Zhao, W.; Quinn, J.; Rafailovich, M. H.; Sokolov, J.; Lennow, R. B.; Eisenberg, A.; Wu, X. Z.; Kim, M. W.; Sinha, S. K.; Tolan, M. *Langmuir* **1995**, *11*, 4785.
(46) Noever, D. A. *Langmuir* **1992**, *8*, 1036.
(47) Molau, G. E. In *Block Copolymers*; Aggarwal, S. L., Ed.; Plenum Press: New York, 1970; p 102.
(48) Hasegawa, H.; Tanaka, H.; Yamasaki, K.; Hashimoto, T. *Macromolecules* **1987**, *20*, 1641.
(49) Herman, D. S.; Kinning, D. J.; Thomas, E. L.; Fetters, L. J. *Macromolecules* **1987**, *20*, 2940.
(50) Ailhaud, H.; Gallot, Y.; Skoulios, A. *Makromol. Chem.* **1972**, *151*, 1.
(51) Lu, J. R.; Su, T. J.; Thomas, R. K.; Penfold, J.; Richards, R. W. *Polymer* **1996**, *37*, 109.
(52) Sauer, B. B.; Yu, H. *Macromolecules* **1989**, *22*, 786.
(53) Alexander, S. *J. Phys.* **1977**, *38*, 983.
(54) Baekmark, T. R.; Elender, G.; Lasic, D. D.; Sackmann, E. *Langmuir* **1995**, *11*, 3975.
(55) Daoud, M.; Cotton, J. *J. Phys.* **1982**, *43*, 531.
(56) Milner, S. T.; Witten, T. A.; Cates, M. E. *Macromolecules* **1988**, *21*, 2610.

MA9802935